

RESOLVING THE CLUMPY STRUCTURE OF THE OUTFLOW WINDS IN THE GRAVITATIONALLY LENSED QUASAR SDSS J1029+2623¹

TORU MISAWA², NAOHISA INADA³, MASAMUNE OGURI^{4,5,6}, POSHAK GANDHI^{7,8}, TAKASHI HORIUCHI⁹, SUZUKA KOYAMADA⁹, RINA OKAMOTO⁹
 misawatr@shinshu-u.ac.jp
 October 6, 2014

ABSTRACT

We study the geometry and the internal structure of the outflowing wind from the accretion disk of a quasar by observing multiple sightlines with the aid of strong gravitational lensing. Using Subaru/HDS, we performed high-resolution ($R \sim 36,000$) spectroscopic observations of images A and B of the gravitationally lensed quasar SDSS J1029+2623 (at $z_{em} \sim 2.197$) whose image separation angle, $\theta \sim 22''.5$, is the largest among those discovered so far. We confirm that the difference in absorption profiles in the images A and B discovered by Misawa et al. (2013) remains unchanged since 2010, implying the difference is not due to time variability of the absorption profiles over the delay between the images, $\Delta t \sim 744$ days, but rather due to differences along the sightlines. We also discovered time variation of C IV absorption strength in both images A and B, due to change of ionization condition. If a typical absorber's size is smaller than its distance from the flux source by more than five orders of magnitude, it should be possible to detect sightline variations among images of other smaller separation, galaxy-scale gravitationally lensed quasars.

Subject headings: quasars: absorption lines — quasars: individual (SDSS J1029+2623)

1. INTRODUCTION

Outflowing winds from accretion disks, accelerated by radiation force (Murray et al. 1995; Proga, Stone, & Kallman 2000), magnetocentrifugal force (Everett 2005; de Kool & Begelman 1995), and/or thermal pressure (Balsara & Krolik 1993; Krolik & Kriss 2001; Chelouche & Netzer 2005), are a key evolutionary link between quasars and their host galaxies. The disk outflow plays an important role as 1) it extracts angular momentum from the accretion disk, leading to growth of black holes (Blandford & Payne 1982; Konigl & Kartje 1994; Everett 2005), 2) it provides energy and momentum feedback and inhibits star formation activity (e.g., Springel, Di Matteo, & Hernquist 2005), and 3) it induces metal enrichment of intergalactic medium (IGM) (Hamann et al. 1997a; Gabel et al. 2006). Outflowing matter has been detected through blueshifted absorption lines in $\sim 70\%$ of quasar spectra (Hamann et al. 2012). These are usually classified as *intrinsic* absorption lines, and distinguished from *intervening* absorption lines that originate in foreground galaxies or in the IGM. Thus, intrinsic absorption lines are powerful and unique tool to probe the outflows in quasars. However, the main challenge in their study is that these are traceable along *only*

single sight-lines (i.e., a one dimensional view alone) toward the nucleus for each quasar, whereas the absorber's physical conditions likely depend strongly on polar angle (e.g., Ganguly et al. 2001; Elvis 2000).

Multiple images of quasars produced by the gravitational lensing effect provide a unique pathway for studying the multiple sightlines, a technique frequently applied for intervening absorbers (e.g., Crotts & Fang 1998; Rauch et al. 1999; Lopez et al. 2005). It is clear that lensed quasars with larger image separation angles have more chance of detecting structural differences in the outflow winds in the vicinity of the quasars themselves. In this sense, the following three lensed quasars are the most promising site for our study as they are lensed by a cluster of galaxies rather than a single massive galaxy: SDSS J1004+4112 with separation angle of $\theta \sim 14''.6$ (Inada et al. 2003), SDSS J1029+2623 with $\theta \sim 22''.5$ (Inada et al. 2006; Oguri et al. 2008), and SDSS J2222+2745 with $\theta \sim 15''.1$ (Dahle et al. 2013). Green (2006) proposed that the differences in emission line profiles between the lensed images of SDSS J1004+4112 can be explained by differential absorptions along each sight-line although no absorption features are detected.

There are clear absorption features detected at the blue wings of the C IV, N V, and Ly α emission lines

¹ Based on data collected at Subaru Telescope, which is operated by the National Astronomical Observatory of Japan.

² School of General Education, Shinshu University, 3-1-1 Asahi, Matsumoto, Nagano 390-8621, Japan

³ Department of Physics, Nara National College of Technology, Yamatokohriyama, Nara 639-1080, Japan

⁴ Research Center for the Early Universe, University of Tokyo, 7-3-1 Hongo, Bunkyo-ku, Tokyo 113-0033, Japan

⁵ Department of Physics, University of Tokyo, 7-3-1 Hongo, Bunkyo-ku, Tokyo 113-0033, Japan

⁶ Kavli Institute for the Physics and Mathematics of the Universe (Kavli IPMU, WPI), University of Tokyo, Chiba 277-8583, Japan

⁷ Department of Physics, Durham University, South Road, Durham DH1 3LE, UK

⁸ Institute of Space and Astronautical Science (ISAS), Japan Aerospace Exploration Agency, 3-1-1 Yoshinodai, chuo-ku, Sagami-hara, Kanagawa 252-5210, Japan

⁹ Department of Physics, Faculty of Science, Shinshu University, 3-1-1 Asahi, Matsumoto, Nagano 390-8621, Japan

¹⁰ The quasar redshift was derived from Mg II emission lines in Inada et al. (2006). An uncertainty of z_{em} is $\Delta z \sim 0.0003$, corresponding to $\Delta v \sim 30$ km s⁻¹. The z_{em} could be blueshifted from the systemic redshift by ~ 100 km s⁻¹ in average (Tytler & Fan 1992).

of other lensed quasar, SDSS J1029+2623 at $z_{em} \sim 2.197^{10}$, the current record-holding large-separation quasar lens, in low/medium resolution spectra (Inada et al. 2006; Oguri et al. 2008). Misawa et al. (2013) obtained high-resolution spectra of the brightest two images (i.e., images A and B), and carefully deblended the C iv and N v absorption lines into multiple narrower components. They show several clear signs supporting an origin in the outflowing wind rather than in foreground galaxies or the IGM (Misawa et al. 2013): i) partial coverage, i.e., the absorbers do not cover the background flux source completely along our sightline, ii) line-locking, iii) large velocity distribution ($\text{FWHM} \geq 1000 \text{ km/s}$), and iv) a small ejection velocity¹¹ from the quasar. Misawa et al. (2013) also discovered a clear difference in parts of these lines between the images A and B in all C iv, N v, Ly α absorption lines, which can be explained by the following two scenarios: (a) intrinsic time variability of the absorption features over the time delay of the two images (e.g., Chartas et al. 2007), and (b) a difference in the absorption levels between the different sight-lines of the outflowing wind (e.g., Chelouche 2003; Green 2006). With a single epoch observation, we cannot distinguish these scenarios.

In this letter, we present results from new spectroscopic observations of SDSS J1029+2623 conducted ~ 4 years later with the goal of conclusively determining the origin of the difference in the absorption features. We also examine the global and internal structure of the outflow. Observations and data reduction are described in §2, and results and discussion are in §3 and §4.

2. OBSERVATIONS AND DATA REDUCTION

We observed the images A and B of SDSS J1029+2623 with Subaru/HDS on 2014 April 4 (the 2014 data, hereafter), 1514 days after the previous observation on February 2010 (the 2010 data; Misawa et al. 2013). The time interval between the observations is longer than the time delay between images A and B, $\Delta t \sim 744$ days in the sense of A leading B (Fohlmeister et al. 2013). We have taken high-resolution spectra ($R \sim 36,000$) with a slit width of $1''.0$, while Misawa et al. (2013) took $R \sim 30,000$ spectra using $1''.2$ slit width. The wavelength coverage is 3400–4230 Å on the blue CCD and 4280–5100 Å on the red CCD, which covers Ly α , N v, Si iv, and C iv absorption lines at $z_{abs} \sim z_{em}$. We also sampled every 4 pixels in both spatial and dispersion directions (i.e., $\sim 0.05\text{Å}$ per pixel) to increase S/N ratio. The total integration time is 11400 s and the final S/N ratio is about 14 pix^{-1} for both of the images.

We reduced the data in a standard manner with the software IRAF¹². Wavelength calibration was performed using a Th-Ar lamp. We applied flux calibrations for quasar spectra using the spectrophotometric standard star Feige34¹³. We did not adjust a spectral resolution of the 2014 spectra ($R \sim 36,000$) to the 2010 ones ($R \sim$

30,000) before comparing them, because a typical line width of each absorption component after deblending into multiple narrower components is large enough ($\text{FWHM} \geq 10 \text{ km s}^{-1}$; Misawa et al. 2013) to ignore the influence of spectral resolution.

3. RESULTS

Here, we examine the time variability of Ly α , N v, and C iv lines. Although Si iv is also detected, we cannot use it for the analysis because the Si iv line is severely contaminated by intervening Si ii and C iv lines at lower redshift. For the purpose of comparing absorption profiles, we increase the S/N ratio by resampling the spectra every 0.5Å . For a more quantitative test, we also compare the flux difference between the two spectra to 3σ flux uncertainty¹⁴.

As shown in Figure 1, we did not find any time variations either in Ly α or N v absorption lines. But C iv lines in both of the images A and B showed clear variation in its line *strength* by more than the 3σ level, without any change in line *profiles*.

In the 2010 spectra, Misawa et al. (2013) discovered a clear difference in parts of C iv, N v, and Ly α absorption lines at an ejection velocity of $v_{ej} \sim 0 - 200 \text{ km s}^{-1}$ between the images A and B. The difference still remains at $\geq 3\sigma$ level in the 2014 spectra, except for the C iv absorption lines for which the difference between images A and B is no longer significant (Figure 2). Thus, absorption components at $v_{ej} \sim 0 - 200 \text{ km s}^{-1}$ (shaded regions in Figures 1 and 2) probably have a different origin from the other absorption components, as suggested in Misawa et al. (2013). We call the former and the latter components as Components 1 and 2 (C_1 and C_2 , hereafter), respectively, and distinguish them in the discussion below.

4. DISCUSSION

In this section, we discuss the difference between the images A and B, the origin of the time variation seen in the C iv lines between the 2010 and the 2014 data, and then the detectability of the sightline variation for quasar images with smaller separations, lensed by a single galaxy.

4.1. Difference between the Images A and B

Misawa et al. (2013) presented two plausible scenarios that explain the sightline variation of the C_1 : (a) time variability over the time delay between the images, $\Delta t \sim 744$ days, and (b) the difference in the absorption levels between two sightlines. With our new data, we can reject the first scenario because C_1 is again detected only in the image A as in the 2010 data. If this is due to time variation, the C_1 has to decrease (from the image A to B in 2010), increase (from the image B in 2010 to the image A in 2014), and then decrease again (from the image A to B in 2014), which requires an unlikely fine-tuning. Although sightline variations are often observed in intervening absorption lines (e.g., Crotts & Fang 1998;

¹¹ The ejection velocity is defined as positive if the absorption line is blueshifted from the quasar emission redshift.

¹² IRAF is distributed by the National Optical Astronomy Observatories, which are operated by the Association of Universities for Research in Astronomy, Inc., under cooperative agreement with the National Science Foundation.

¹³ We reduced the 2010 data again by applying flux calibration, while Misawa et al. (2013) only presented normalized spectra. Because the continuum fitting gives an additional uncertainty for absorption depth and profile we use flux-calibrated spectra in this study.

¹⁴ Total flux uncertainty is calculated by $\sigma = \sqrt{\sigma_1^2 + \sigma_2^2}$, where σ_1 and σ_2 are the one sigma errors of the first and second spectra, respectively, and include photon-noise and readout-noise.

Rauch et al. 1999; Lopez et al. 2005), the C_1 in the image A should have its origin in *intrinsic* absorber because it shows partial coverage (Misawa et al. 2013) and time variation (this study). Thus, the geometry of the outflow is such that the C_1 covers only sightline to the image A, while the C_2 covers both sightlines of the images A and B.

A possible structure of the outflow is shown in Figure 3. The C_1 absorber covers only the sightline toward image A but not image B, regardless of its distance (r) from the flux source. The size of the absorbing cloud (d_{cloud}) should be smaller than the size of the flux source (because of partial coverage) and also smaller than the physical distance between the sightlines of the lensed images, i.e., $d_{cloud} \leq r\theta$ to avoid covering both sightlines. Here, we assume the separation angle of the two sightlines from the flux source is very similar to that seen from us. On the other hand, C_2 has two possible origins: a) small gas clouds close to the flux source and b) filamentary (or sheet-like) structure made of multiple clumpy gas clouds (Misawa et al. 2013). In either case, both sightlines A and B need to be covered. We will discuss these further in Section 4.3.

4.2. Origin of Time Variation in C IV Lines

Time variability is frequently detected in broad absorption lines (BALs) with line widths of $\geq 2,000 \text{ km s}^{-1}$ (e.g., Gibson et al. 2008; Capellupo et al. 2013; Trevese et al. 2013). Some narrower intrinsic absorption lines (NALs and mini-BALs) are also known to be variable (e.g., Wise et al. 2004; Narayanan et al. 2004; Misawa et al. 2014). There are several explanations for the time variation, including gas motion across our line of sight (e.g., Hamann et al. 2008; Gibson et al. 2008), changes of the ionization condition (e.g., Hamann et al. 2011; Misawa et al. 2007b), and a variable scattering material that redirect photons around the gas clouds (e.g., Lamy & Hutsemékers 2004). These mechanisms are not applicable to intervening absorbers because they have larger sizes (i.e., gas motion and photon redirection do not work) and lower densities (i.e., the variability time scale due to ion recombination is too long to observe over several years), compared to intrinsic absorbers as noted in Narayanan et al. (2004).

In our monitoring campaign, only C IV absorption lines show clear time variation in both of the images. The absorption strength is seen to weaken over the entire wavelength range (see Figure 1). This immediately rejects the gas motion scenario because all gas clouds that produce the C_1 and the C_2 need to cross our sightline in concert, which is highly unlikely. The scattering scenario is also difficult to accept because it cannot explain the fact that only C IV changes while N V and Ly α are stable. Thus, we conclude that the change of ionization scenario is the most plausible explanation.

The C_1 , arising in the absorber that locate only on the sightline A, was monitored twice in 2010 and 2014. On

the other hand, the C_2 has two possibilities. If the corresponding absorber locates on both sightlines toward the images A and B, we have monitored the variable C IV lines in four epochs, i.e., images A and B in 2010 and then images A and B in 2014, with time intervals of ~ 744 , 770, and 744 days, given the time delay of $\Delta t = 744$ days between images A and B. If the filamentary (or sheet-like) structure is the case, it means we have monitored them only twice as we did for the C_1 . In either case, we cannot monitor the ionization condition of the absorbers because a wide range of ionic species (which is necessary for photoionization modeling) are not detected in our spectra.

Here, we discuss two possible scenarios for explaining the decrease of the C IV line strength. First, the ionization level may have increased between the observations with more C^{3+} ionized to C^{4+} while the ionization fraction of N^{4+} remained stable. If the absorber's ionization parameter¹⁵ is $\log U \sim -1.5$, at which point the ionization fraction of N V is close to peak (Hamann 1997), this scenario is possible¹⁶. Alternatively, the invariance of N V may be due to the saturation effect with partial coverage. Another possible interpretation is recombination of C^{3+} to C^{2+} . In this case, we can place constraints on the electron density and the distance from the flux source by the same prescription as used in Narayanan et al. (2004), assuming the variation time scale as the upper limit of the recombination time. If we monitored the absorbers twice (i.e., C_1 and C_2 in the filamentary model) or four times (i.e., C_2 in the single-sightline model), the electron density is estimated to be $n_e \geq 8.7 \times 10^3 \text{ cm}^{-3}$ or $1.72 \times 10^4 \text{ cm}^{-3}$, and the distance from the flux source to be $r \leq 620 \text{ pc}$ or 440 pc , respectively. Because the absorber's distance is always smaller than the boundary distance (see Section 4.3) in both cases, the filamentary model can be rejected for the C_2 if recombination is the origin of the variation.

4.3. Detectability of Sightline Difference

Whether we detect sightline difference or not depends on the absorber's size and its distance from the flux source. For placing constraints on the absorber's distance, the size estimation of the background flux source is very important. The outflow wind in SDSS J1029+2623 probably covers both the continuum source with a size of $R_{cont} \sim 2.5 \times 10^{-4} \text{ pc}^{17}$ and broad emission-line region (BELR) with a size of $R_{BELR} \sim 0.09 \text{ pc}^{18}$ because the residual flux at the bottom of the absorption lines are close to zero around the peak of the broad emission lines (i.e., covering factor toward BELR is $C_f \sim 1$). Following Misawa et al. (2013), we define a boundary distance (r_b), a distance from the flux source where the physical distance between two sightlines ($r_b\theta$) is same as R_{BELR} (i.e., the two sightlines become fully separated with no overlap at $r > r_b$). If the BELR as well as the continuum source is the background source, the boundary distance is $r_b \sim 788 \text{ pc}^{19}$.

Here, we present two possible scenarios for the origin of

¹⁵ The ionization parameter U is defined as the ratio of hydrogen ionizing photon density (n_γ) to the electron density (n_e), $U \sim n_\gamma/n_e$.

¹⁶ For example, the ionization fraction of C^{3+} changes by a factor of ~ 2 while the corresponding change is only $\sim 5\%$ for N^{4+} with a variation of $\Delta \log U \sim 0.3$ around $\log U \sim -1.5$, assuming the continuum shape of typical quasar used in Narayanan et al. (2004).

¹⁷ We assume R_{cont} is five times the Schwarzschild radius, $R_{cont} = 10GM_{BH}/c^2$.

¹⁸ This is calculated in Misawa et al. (2013), using the empirical relation between R_{BELR} and quasar luminosity (Kaspi et al. 2000; McLure & Dunlop 2004).

¹⁹ If only the continuum source is the background source, which is applicable for absorption lines with large ejection velocity, the boundary distance is $r_b \sim 2.3 \text{ pc}$.

the C_1 . First, the C_1 absorber could locate at larger distance than the boundary distance, ≥ 788 pc. In this case, the C_1 absorber may be the inter-stellar medium (ISM) of the host galaxy that are swept up by an accretion disk wind (Kurosawa & Proga 2009). Another possible scenario is that the absorber could be small clumpy cloud that locate at the outskirts of the C_2 absorber whose distance is smaller than the boundary distance. Hamann et al. (2013) suggests that mini-BAL absorbers consist of a number of small gas clouds ($d_{\text{cloud}} \leq 10^{-3} - 10^{-4}$ pc) with very large gas density ($n_e \geq 10^6 - 10^7 \text{ cm}^{-3}$) at the absorber's distance of $r \sim 2$ pc to avoid over-ionization. A similar picture is also suggested for BAL quasars (Joshi et al. 2014). Furthermore, recent radiation-MHD simulations by Takeuchi et al. (2013) reproduce variable clumpy structures with typical sizes of $\sim 20 r_g$ in warm absorbers, corresponding to $\sim 5 \times 10^{-4}$ pc assuming the black-hole mass of SDSS J1029+2623, $M_{\text{BH}} \sim 10^{8.72} M_{\odot}$. Indeed, high-velocity intrinsic NALs are frequently detected with partial coverage toward the continuum source only, sug-

gesting their typical size is comparable to or smaller than the continuum source (Misawa et al. 2007a).

Our results have broader implications as well. Figure 4 summarizes physical distance between lensed images as a function of separation angle for the 124 lensed quasars discovered to date²⁰, assuming the absorber's distance is 1 pc, 10 pc, 100 pc, and 1 kpc. The sightline difference will be detected for quasars lensed by a single galaxy whose typical separation angle is $\theta \sim 2''$, if the absorber's size is smaller than its distance from the flux source by more than five orders of magnitude (i.e., $d_{\text{cloud}}/r \leq \theta$). This would place an important constraint on the absorbers.

We thank the anonymous referee for a number of comments that helped us improve the paper. We also thank Koji Kawabata and Akito Tajitsu for their comments about data analysis. The research was supported by JGC-S Scholarship Foundation, and partially supported by the Japan Society for the Promotion of Science through Grant-in-Aid for Scientific Research 26800093.

REFERENCES

- Balsara, D. S., & Krolik, J. H. 1993, *ApJ*, 402, 109
 Blandford, R. D., & Payne, D. G. 1982, *MNRAS*, 199, 883
 Capellupo, D. M., Hamann, F., Shields, J. C., Halpern, J. P., & Barlow, T. A. 2013, *MNRAS*, 429, 1872
 Chartas, G., Eracleous, M., Dai, X., Agol, E., & Gallagher, S. 2007, *ApJ*, 661, 678
 Chelouche, D., & Netzer, H. 2005, *ApJ*, 625, 95
 Chelouche, D. 2003, *ApJ*, 596, L43
 Crotts, A. P. S., & Fang, Y. 1998, *ApJ*, 502, 16
 Dahle, H., Gladders, M. D., Sharon, K., et al. 2013, *ApJ*, 773, 146
 de Kool, M., & Begelman, M. C. 1995, *ApJ*, 455, 448
 Elvis, M. 2000, *ApJ*, 545, 63
 Everett, J. E., 2005, *ApJ*, 631, 689
 Fohlmeister, J., Kochanek, C. S., Falco, E. E., et al. 2013, *ApJ*, 764, 186
 Gabel, J. R., Arav, N., & Kim, T.-S. 2006, *ApJ*, 646, 742
 Ganguly, R., Bond, N. A., Charlton, J. C., Eracleous, M., Brandt, W. N., & Churchill, C. W., 2001, *ApJ*, 549, 133
 Gibson, R. R., Brandt, W. N., Schneider, D. P., & Gallagher, S. C. 2008, *ApJ*, 675, 985
 Green, P. J. 2006, *ApJ*, 644, 733
 Hamann, F., Chartas, G., McGraw, S., et al. 2013, *MNRAS*, 435, 133
 Hamann, F., Simon, L., Hidalgo, P. R., & Capellupo, D. 2012, *AGN Winds in Charleston*, 460, 47
 Hamann, F., Kanekar, N., Prochaska, J. X., et al. 2011, *MNRAS*, 410, 1957
 Hamann, F., Kaplan, K. F., Rodríguez Hidalgo, P., Prochaska, J. X., & Herbert-Fort, S. 2008, *MNRAS*, 391, L39
 Hamann, F. 1997, *ApJS*, 109, 279
 Hamann, F., Barlow, T. A., Junkkarinen, V., & Burbidge, E. M., 1997, *ApJ*, 478, 80
 Inada, N., Oguri, M., Morokuma, T., et al. 2006, *ApJ*, 653, L97
 Inada, N., Oguri, M., Pindor, B., et al. 2003, *Nature*, 426, 810
 Joshi, R., Chand, H., Srianand, R., & Majumdar, J. 2014, *MNRAS*, 442, 862
 Kaspi, S., Smith, P. S., Netzer, H., et al. 2000, *ApJ*, 533, 631
 Konigl, A., & Kartje, J. F. 1994, *ApJ*, 434, 446
 Krolik, J. H., & Kriss, G. A. 2001, *ApJ*, 561, 684
 Kurosawa, R. & Proga, D. 2009, *ApJ*, 693, 1929
 Lamy, H., & Hutsemékers, D. 2004, *A&A*, 427, 107
 Lopez, S., Reimers, D., Gregg, M. D., et al. 2005, *ApJ*, 626, 767
 McLure, R. J., & Dunlop, J. S. 2004, *MNRAS*, 352, 1390
 Misawa, T., Charlton, J. C., & Eracleous, M. 2014, *ApJ*, 792, 77
 Misawa, T., Inada, N., Ohsuga, K., et al. 2013, *AJ*, 145, 48
 Misawa, T., Charlton, J. C., Eracleous, M., et al. 2007a, *ApJS*, 171, 1
 Misawa, T., Eracleous, M., Charlton, J. C., & Kashikawa, N. 2007b, *ApJ*, 660, 152
 Murray, N., Chiang, J., Grossman, S. A., & Voit, G. M., 1995, *ApJ*, 451, 498
 Narayanan, D., Hamann, F., Barlow, T., Burbidge, E. M., Cohen, R. D., Junkkarinen, V., & Lyons, R., 2004, *ApJ*, 601, 715
 Oguri, M., Ofek, E. O., Inada, N., et al. 2008, *ApJ*, 676, L1
 Proga, D., Stone, J. M., & Kallman, T. R., 2000, *ApJ*, 543, 686
 Rauch, M., Sargent, W. L. W., & Barlow, T. A. 1999, *ApJ*, 515, 500
 Springel, V., Di Matteo, T., & Hernquist, L. 2005, *ApJ*, 620, L79
 Takeuchi, S., Ohsuga, K., & Mineshige, S. 2013, *PASJ*, 65, 88
 Trevese, D., Saturni, F. G., Vagnetti, F., et al. 2013, *A&A*, 557, A91
 Tytler, D., & Fan, X.-M. 1992, *ApJS*, 79, 1
 Wise, J. H., Eracleous, M., Charlton, J. C., & Ganguly, R., 2004, *ApJ*, 613, 20

²⁰ These are collected from the lensed quasar catalogs; CASTLE (<http://www.cfa.harvard.edu/castles>) and SQLS (<http://www.utap.phys.s.u-tokyo.ac.jp/~sdss/sqls>).

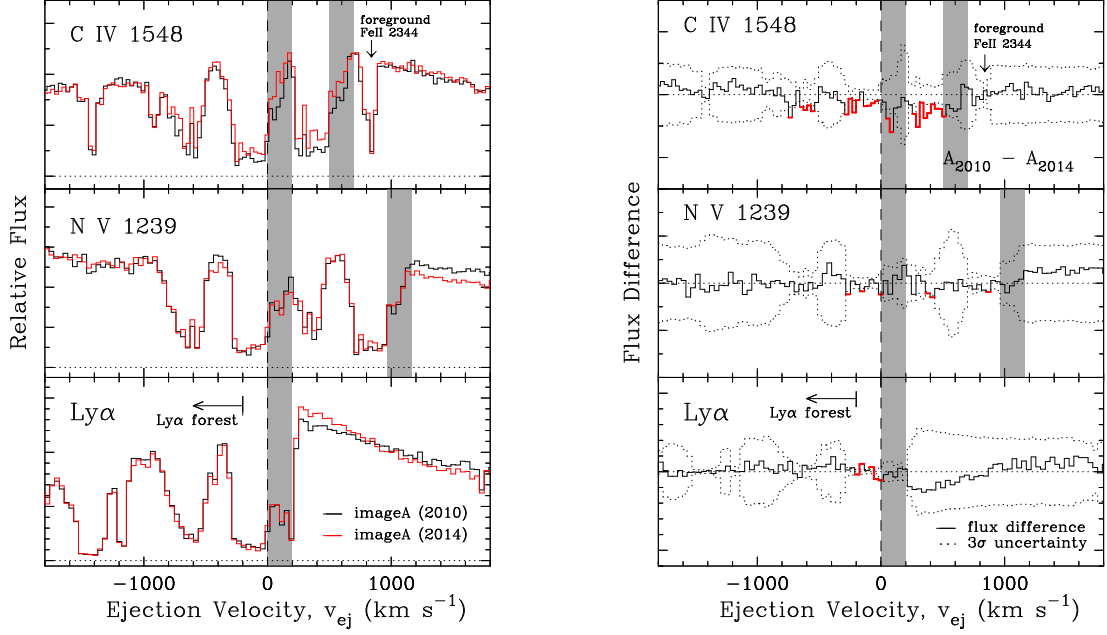


FIG. 1.— Comparison of the C IV, N V, and Ly α absorption profiles taken in 2010 (black) and 2014 (red) toward the image A of SDSS J1029+2623. (Left) The horizontal axis denotes ejection velocity relative to the quasar emission redshift ($z_{em} \sim 2.197$). The vertical axis flux scale is arbitrary. The shaded regions cover the C_1 of Ly α line and the doublets of C IV and N V lines while the other regions are the C_2 . Intervening absorption lines that are not related to the outflow are marked with arrows and transition names. (Right) Comparison of flux difference between two spectra (solid histogram) with flux uncertainty (dotted histogram). Spectral regions where absorption line show variation in more than 3σ level are marked with red histogram, except for Ly α forest and intervening absorption lines.

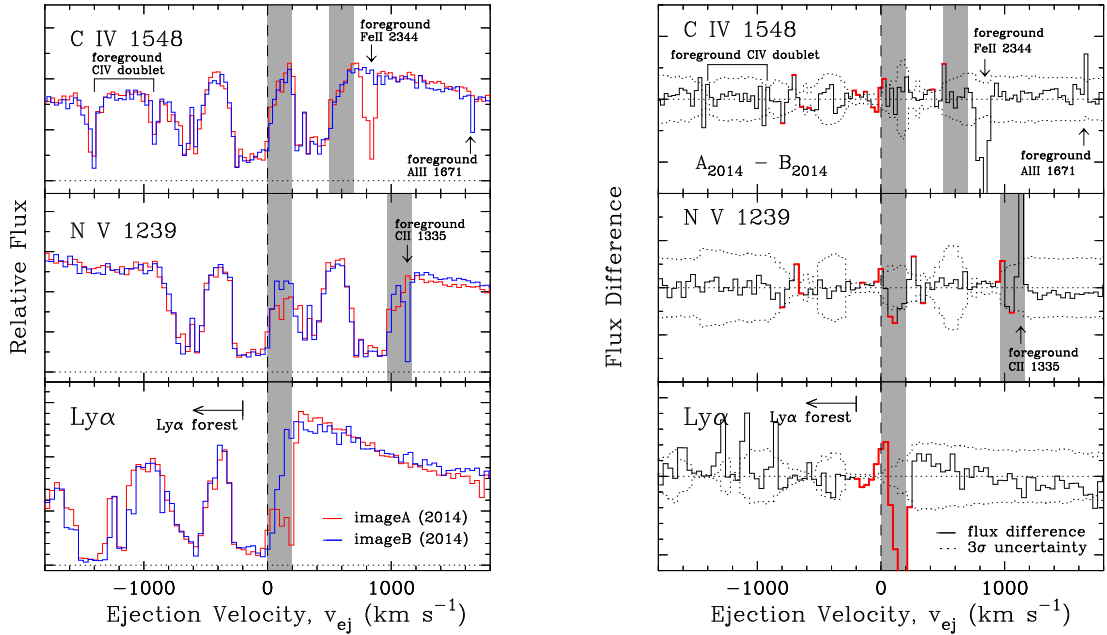


FIG. 2.— Same as Figure 1 but for the images A (red) and B (blue) of the 2014 spectra. The C IV doublet at $v_{ej} \sim -1400$ km s⁻¹, which shows $\geq 3\sigma$ difference, is probably an intervening absorption line because the profile is narrow and the flux at the line center approaches close to zero before sampling. The profile difference in the shaded regions between the images A and B detected in the 2010 data (Misawa et al. 2013) still remains in the 2014 data.

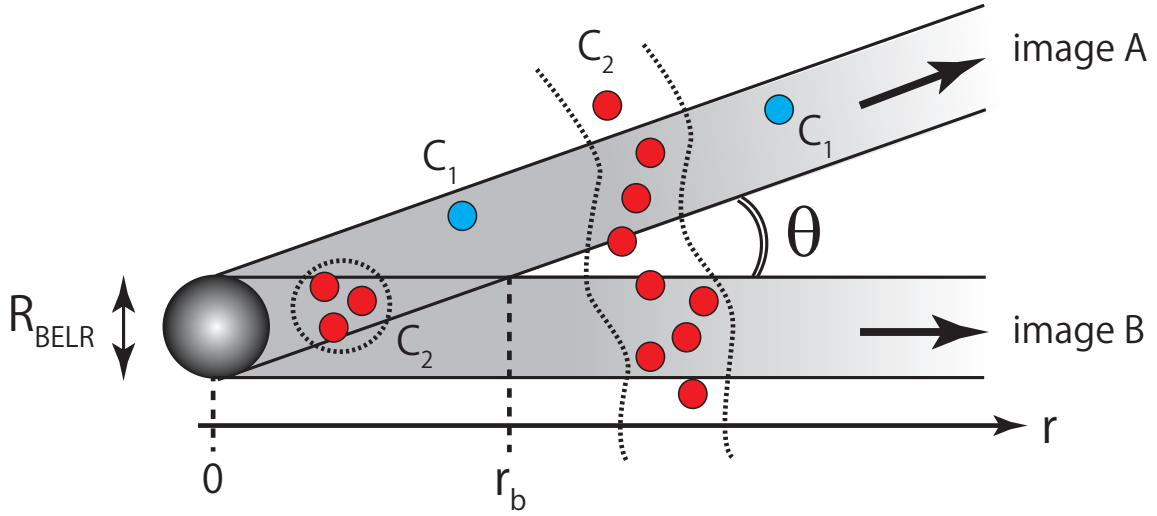


FIG. 3.— Possible locations of the C_1 and C_2 absorbers toward our sightlines. The large sphere represents the broad emission line region as a background flux source, while small blue and red filled circles are the C_1 and C_2 absorbers. The C_1 absorber always locates on only the sightline toward the image A, regardless of its distance. C_2 locates on both sightlines toward the images A and B or has a filamentary (or sheet-like) structure consisting of number of small clumpy clouds. The boundary distance (r_b) is the distance at which the two sightlines become fully separated with no overlap.

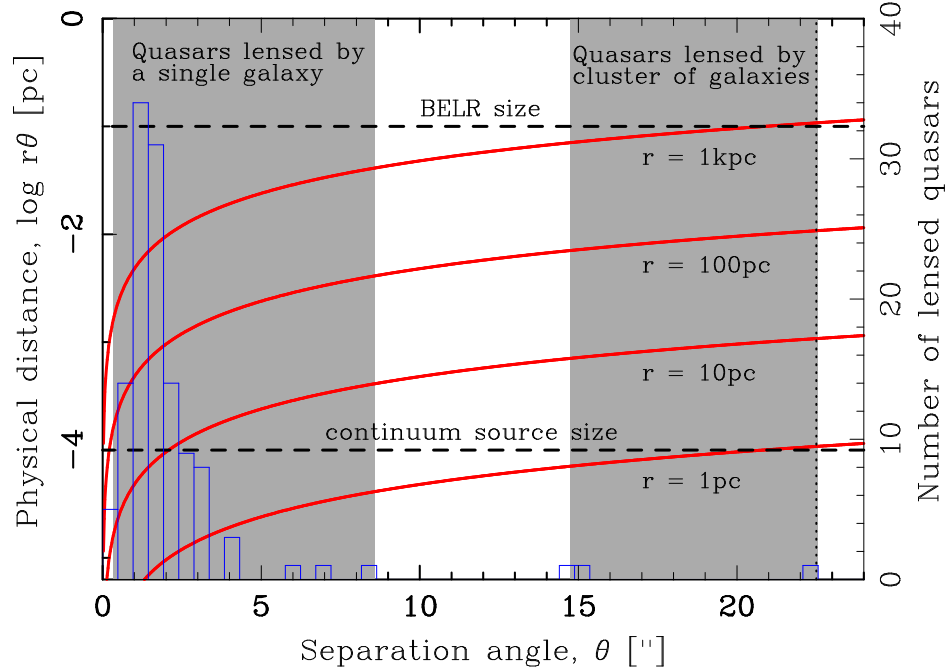


FIG. 4.— Physical distance between two sightlines of lensed images as a function of separation angle (red curves), adopting the absorber's distance of $r = 1, 10, 100$, and 1000 pc. The horizontal dotted lines mark sizes of BELR (~ 0.1 pc) and the continuum source ($\sim 10^{-4}$ pc) of SDSS J1029+2623. The histogram denotes the distribution of separation angles of 124 lensed quasars that have been discovered to date. Shaded regions are ranges of separation angles of quasar images lensed by a single galaxy or by a cluster of galaxies.